LEGIBILITY NOTICE

A major purpose of the Technical Information Center is to provide the broadest dissemination possible of information contained in DOE's Research and Development Reports to business, industry, the academic community, and federal, state and local governments.

Although a small portion of this report is not reproducible, it is being made available to expedite the availability of information on the research discussed herein.

CONF 8606202--3

LA-UR-86-3340

Los Alamos National Laboratory is operated by the University of California for the United States Department of Energy under contract W-7405-ENG-36.

LA-UR--86-3340

DE87 000166

TITLE: HYDRODYNAMIC EFFECTS IN EVAPORATING DROPLETS

AUTHOR(S): ROBERT L. ARMSTRONG, NMSU
ANDREW ZARDECKI, T-DOT

SUBMITTED TO: PROCEEDINGS OF THE 1986 CRDEC SCIENTIFIC CONFERENCE ON OBSCURATION AND AEROSOL RESEARCH

DISCLAIMER

SEPT. 25, 1986

MASTER

Los Alamos Los Alamos National Laboratory
Los Alamos, New Mexico 87545

FORM NO 836 R4
ST NO 2629 5/81

HYDRODYNAMIC EFFECTS IN EVAPORATING DROPLETS

R. L. Armstrong, Physics Department, Applied Laser Optics Group
New Mexico State University
Las Cruces, New Mexico 88003

and

A. Zardecki, Theoretical Division
Los Alamos National Laboratory
Los Alamos, New Mexico 87545

RECENT PUBLICATIONS AND PRESENTATIONS:

A) R. L. Armstrong, S. A. W. Gerstl, and A. Zardecki, "On the Propagation of Intense Optical Beams Through Vaporizing Aerosols", paper presented at 1985 CRDC Conference on Obscuration and Aerosol Research.

B) R. L. Armstrong, S. A. W. Gerstl, and A. Zardecki, "Non-linear Pulse Propagation in the Presence of Evaporating Aerosols", J. Opt. Soc. Am. A2, 1739 (1985).

C) R. L. Armstrong, P. J. O'Rourke, and A. Zardecki, "Vaporization of Irradiated Droplets", to be published in Physics of Fluids.

ABSTRACT

The vaporization of a spherically symmetric liquid droplet homogeneously heated by a high-intensity laser pulse is investigated on the basis of a hydrodynamic description of the system composed of the vapor and ambient gas. In the limit of convective vaporization, the boundary conditions at the fluid-gas interface are formulated by using the notion of a Knudsen layer across which translational equilibrium is established. Numerical solutions to the hydrodynamic equations exhibit the existence of two shock waves propagating in opposite directions with respect to the contact discontinuity that separates the ambient gas and vapor.

I. Introduction

A wide variety of effects can influence the evaporation of aerosol droplets by intense electromagnetic radiation. The evaporation of a droplet by irradiation with a long pulse of low energy is controlled by the processes of heat conduction and vapor diffusion. This case of isobaric vaporization, in which a pressure wave induced in the surrounding gas in response to the mass and heat addition can be neglected, is fairly straight-forward and lends itself to detailed numerical computations.[1-3] However, when a droplet is irradiated with a short pulse of high energy density, the resulting phenomena are more complex and more difficult to treat theoretically. With convective evaporation being a dominant process, sufficiently large droplets will undergo explosive vaporization,[4-5] creating shock waves. Typically, when the droplet radius does not exceed 10 μm and the incident-flux level is in the range of 10^3-10^5 W/cm^2, diffusive evaporation is dominant; for fluxes reaching 10^7 W/cm^2 the evaporation becomes convective and shock formation is important. The experiments of Kafalas et al.[6-7] provide classic examples of shock waves produced by explosive vaporization.

In this paper we extend a previous analysis[8] of low mass-flux vaporization produced by low-irradiance pulsed beams to the case of high-irradiance submicrosecond pulses where the low mass flux hypothesis can no longer by justified. In terms of the droplet-radius vs. beam-irradiance phenomenology regimes discussed by Reilly[9], the convective mass flux regime will be analyzed in this paper. We do not treat the higher irradiance regime for which the droplet shattering and fast ablation processes become significant.

II. Hydrodynamic Description

In this section, we formulate the hydrodynamical description for the vapor and ambient gas in the region external to the evaporating droplet. The assumption that the conditions on the droplet surface are uniform (uniform heating of the droplet by the radiation), supplemented by the Knudsen layer jump conditions[10] at the droplet boundary, leads to a complete droplet phase change model. The jump conditions for the temperature and the vapor density are found to be a function of the vapor Mach number, a free parameter in Knight's analysis.[10] Knight determines the Mach number for the case of an idealized flow field adjacent to a vaporizing surface. For the present problem of an evaporating droplet, the flow becomes non-uniform at later

times as the initial shock wave weakens. For intense irradiation, however, the flow becomes supersonic at early times and it may be shown[11] that, under these conditions, the boundary conditions may be determined independently of the external flow field. This implies that the idealized flow field assumed in our model plays a role in the determination of the droplet boundary conditions only for the earliest times where it represents a reasonable approximation. At later times, where the actual flow is markedly different from the idealized flow, the boundary conditions may be determined independently of the idealized flow.

III. Numerical Solutions

We have obtained numerical solutions to the hydrodynamic equations external to an intensely irradiated evaporating droplet. The numerical solution procedure is embodied in the CON1D[12] computer program, which solves these equations by finite difference methods. The solution procedure is based on the ICE (Implicit Continuous-Field Eulerian[13] and the ALE (Arbitrary Lagrangian-Eulerian)[14] numerical methods. The ICE method allows the efficient solution of both low and high Mach number flows with the same computer program. Thus, CON1D can solve both constant pressure evaporation and explosive evaporation cases. The ALE method allows the user great flexibility in moving or rezoning the computational mesh. This flexibility is used in the calculations of this paper to rezone the mesh to follow the receding droplet surface.

We consider the case of evaporating water droplets in an ambient atmosphere, modeled as a mixture of oxygen and nitrogen. The energy deposition is due to a time-dependent radiation flux F, assumed to have the form of a Gaussian laser pulse

$$F(t) = F_{MAX} \exp[-(t - t_o)^2/2t_p^2] \quad , \qquad (1)$$

where F_{MAX} is the peak value of the flux.

Figures 1-6 illustrate the results of CON1D calculations for the case of a 10 μm droplet, with the pulse characterized by the values of $F_{MAX} = 1.52 \times 10^9 W/cm^2$, $t_o = 1.5 \times 10^{-7}$ s, and $t_p = 5.0 \times 10^{-8}$ s; the laser wavelength is 10.6 μm.

Figures 1 and 2 illustrate the spatial dependence of four hydrodynamic variables, the pressure (in logarithmic units), the temperature, the mass-averaged velocity, and the vapor mass fraction. Figure 1 is a snapshot taken at t = 0.224 μs (after 270 cycles), whereas Fig. 2 is taken at t = 0.269 μs (after 330 cycles). Both these cycles correspond to times from the trailing edge of the pulse. In each case, the droplet is at ambient conditions prior to the arrival of the pulse at

t = 0. The radial coordinate is measured from an origin at the surface of the evaporating droplet. For the case of a 10 μm droplet, the radial variable ranges to 20 droplet radii.

The two snapshots shown in Figs. 1 and 2 capture the medium surrounding the irradiated droplet at times when several hydrodynamic features of interest may be identified. These are indicated in Figs. 1 and 2 (on the velocity curves only) by the five letters A through E. Moving outward from the droplet surface, the five regions are: A - region of supersonic expansion; B - backward-facing shock wave; C - transition region separating the backward- from the forward-facing shock wave; D - forward-facing (initial disturbance) shock wave; E - undisturbed medium ahead of forward shock. An inspection of the velocity curves shows the large negative velocity gradients in B and D that indicate the presence of shock waves, and the positive velocity gradient in A that accompanies the supersonic rare-faction fan. The backward-facing shock is a reflected shock that is produced when the supersonically expanding material in region A collides with the high pressure material in region C. Both the forward-facing and reflected shocks are propagating away from the droplet surface (to the right), but the reflected shock may be seen to be propagating to the left relative to the moving vapor in B. The transition region C contains the contact discontinuity and, additionally, exhibits an interesting transition from compression (negative velocity gradient) at $t \leq 0.224$ μs to expansion (positive velocity gradient) at $t \geq 0.269$ μs. The temperature changes occurring in C during this period are in accord with the isentropic nature of this compression and expansion process. We finally note that dispersive errors in the numerical calculations have produced several non-physical computational artifacts, notably the spurious peaks at the A-B boundary of the pressure, temperature, and velocity curves, and the $Y > 1$ region of the mass fraction curves.

Figures 3-6 illustrate the spatio-temporal dependence of the four hydrodynamic variables, p, T, u, and Y, for the same droplet-beam system described in Figs. 1-2. The five regions described in Figs. 1-2 may be readily identified in Figs. 3-6. Notice in particular how the shock structure detaches from the droplet boundary at early times and propagates into the surrounding medium. The backward-facing shock is particularly evident in the temperature plot, Fig. 4. Examination of the velocity plot, Fig. 5, clearly reveals the changes occurring in the transition region C from compression at early times to rare-faction at later times. Finally,

the computational artifacts are evident in these figures as sharp ridges on the otherwise smoothly varying hydrodynamic features.

IV. Conclusions

Under the assumption of homogeneous heating, we have developed a theoretical model for rapid droplet vaporization into the surrounding ambient atmosphere. The equations of hydro-dynamics have been solved in the region adjacent to the droplet in the convective regime, established when the rate of energy deposition is sufficiently high. For 10 μm droplets, this requires the laser flux to exceed 10^7 W/cm^2. At high evaporation rates, the notion of the Knudsen layer enables us to use approximate jump conditions at the droplet-vapor interface. Since the diffusive evaporation remains unaccounted for, our theory does not provide a smooth transition to the low-flux regime. Still, the regime of convective vaporization includes a variety of parameters of practical interest in the plane having laser flux and droplet radius as axes. Within the limitations of our approach, we have found a complex hydrodynamic solution for the system composed of the vapor and ambient gas. In particular, in contrast to a standard description of the propagation of a discontinuity in planar geometry,[15] we have shown the existence, largely because of the spherical geometry, of two shock waves moving in opposite directions with respect to the contact discontinuity surface. These shock waves are separated from the droplet surface by a supersonic rarefaction fan.

Future research should provide a transition to the diffusive vaporization regime, as well as the description of nonuniform heating. Recent experiments of Qian, et al.[16] demonstrate the existence of hot spots inside of the water drops. To accomplish the goals of this program, however, one would need to solve the hydrodynamic equations both inside and outside the droplet. The dynamical coupling between the electromagnetic field and the hydrodynamics is also significant, as has been recently shown by Chitanvis.[17]

REFERENCES

1. F. A. Williams, Combustion Theory (Addison Wesley, Reading, Mass., 1965).
2. R. L. Armstrong, Appl. Opt. 23, 148 (1984).
3. G. Sageev and J. H. Seinfeld, App. Opt. 23, 4368 (1984).
4. V. V. Barinov and S. A. Sorokin, Kvantovaya Electron. 2, 5 (1973) [Sov. J. Quant. Electron. 3, 89 (1973)].

5. V. A. Batanov, F. V. Bunkin, A. M. Prokhorov, and V. B. Fedorov, Zh. Eksp. Teor. Fiz. 63, 586 (1972) [Sov. Phys. JETP 36, 311 (1973)].

6. P. Kafalas and A. P. Ferdinand, Jr. Appl. Opt. 12, 29 (1973).

7. P. Kafalas and J. Herrmann, Appl. Opt. 12, 772 (1973).

8. R. L. Armstrong, S. A. W. Gerstl, and A. Zardecki, J. Opt. Soc. Am. 2. 1739 (1985)

9. T. P. Reilly, Proc. Soc. Photo-Opt. Instrum. Eng. 410, 2 (1983).

10. C. J. Knight, AIAA Journ. 17, 519 (1979).

11. R. L. Armstrong, P. J. O'Rourke and A. Zardecki, to be published in Physics of Fluids.

12. R. D. Janssen and P. J. O'Rourke, "CON1D: A Computer Program for Calculating Spherically Symmetric Droplet Combustion", Los Alamos National Laboratory report LA-10269-MS (December 1984).

13. F. H. Harlow and A. A. Amsden, J. Comput. Phys. 8, 197 (1971).

14. C. W. Hirt, A. A. Amsden, and J. L. Cook, J. Comput. Phys. 14, 227 (1974).

15. Ya. B. Zel'dovich and Yu. P. Raizer, Physics of Shock Waves and High-Temperature Hydrodynamic Phenomena (Academic Press, New York, 1966), p. 84.

16. S. X. Qian, J. B. Snow, and R. K. Chang, Opt. Lett. 10, 499 (1985).

17. S. M. Chitanvis, Physica A, in press, (1986).

FIGURE CAPTIONS

1. Pressure, temperature, velocity, and mass fraction as a function of distance from the center of the drop. The peak laser flux $F_{MAX} = 1.52 \times 10^9$ W/cm^2; pulse width $t_p = 5.0 \times 10^{-8}$ s. The cycle 270 corresponds to the time $t = 0.224 \times 10^{-6}$ s.
2. Same as Fig. 1, but cycle 330 corresponding to $t = 0.269 \times 10^{-6}$ s.
3. Space-time dependence of pressure (logarithmic units).
4. Space-time dependence of temperature.
5. Space-time dependence of mass-averaged velocity.
6. Space-time dependence of vapor mass fraction.

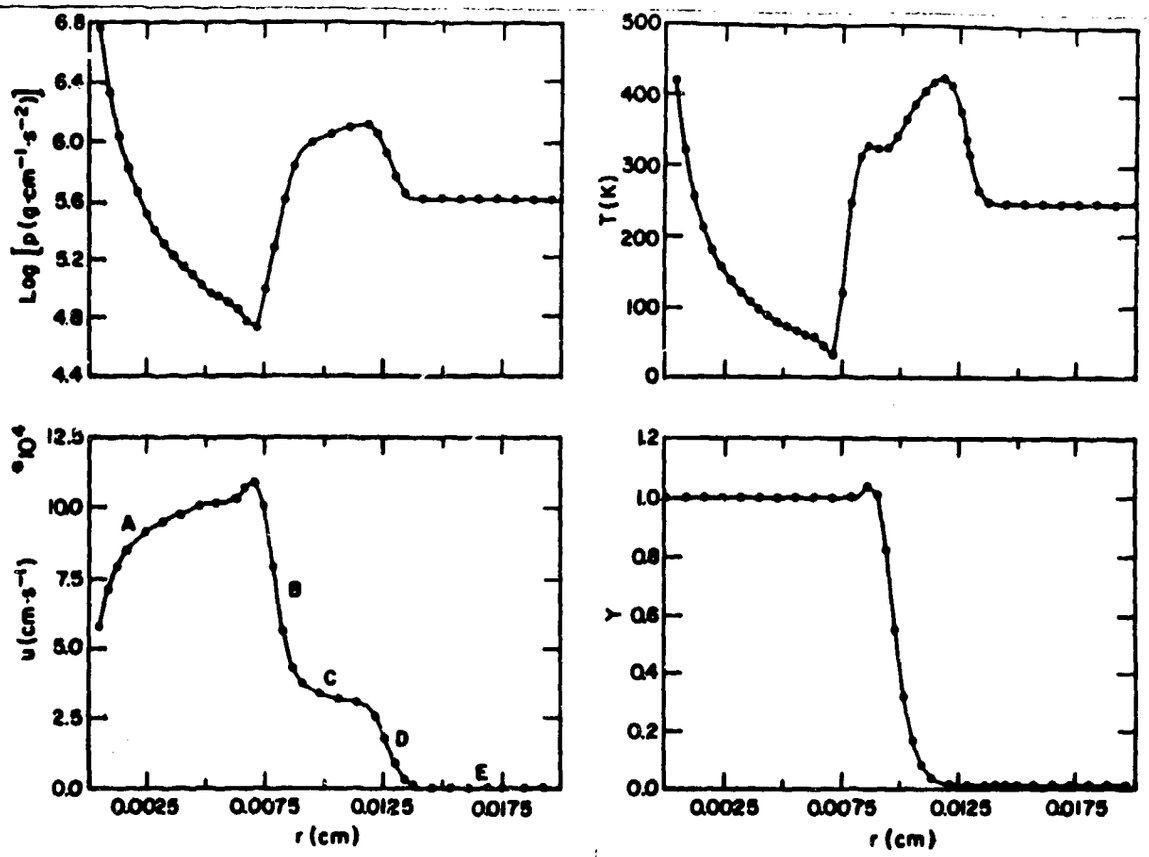

FIGURE 1

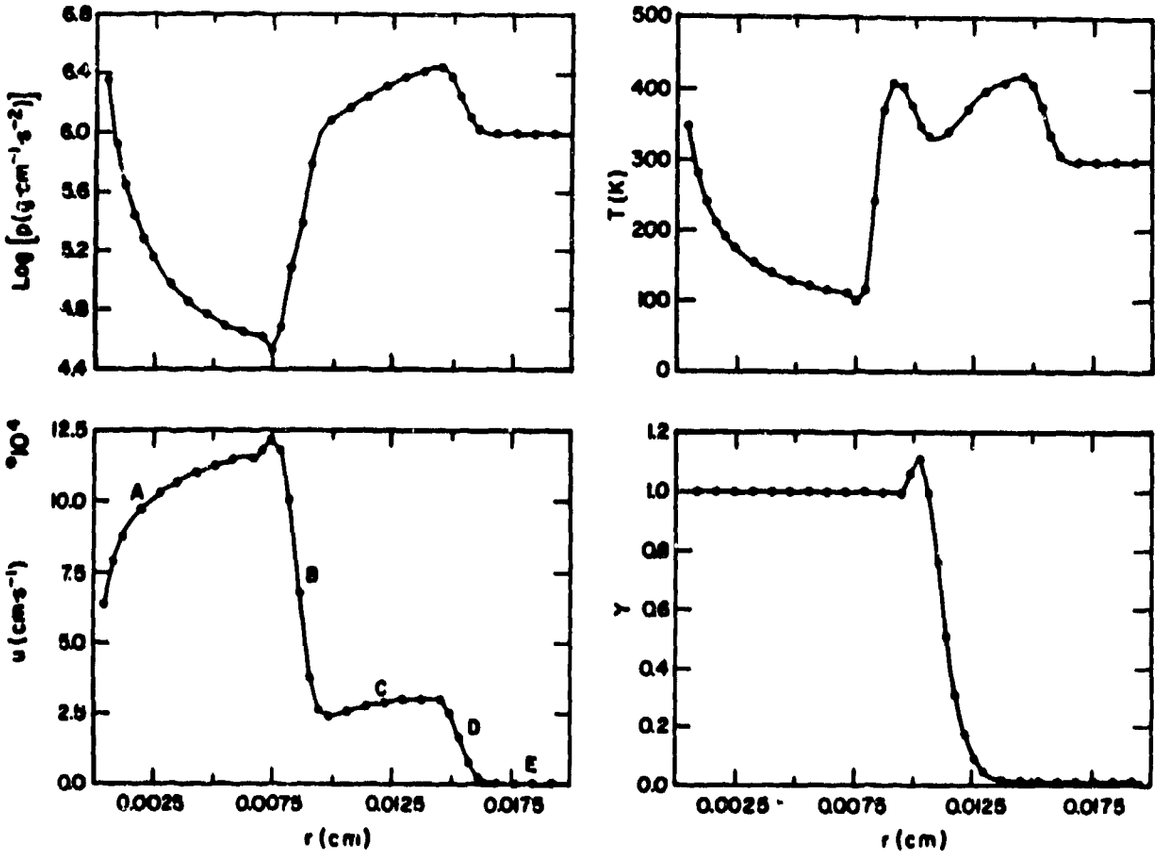

FIGURE 2

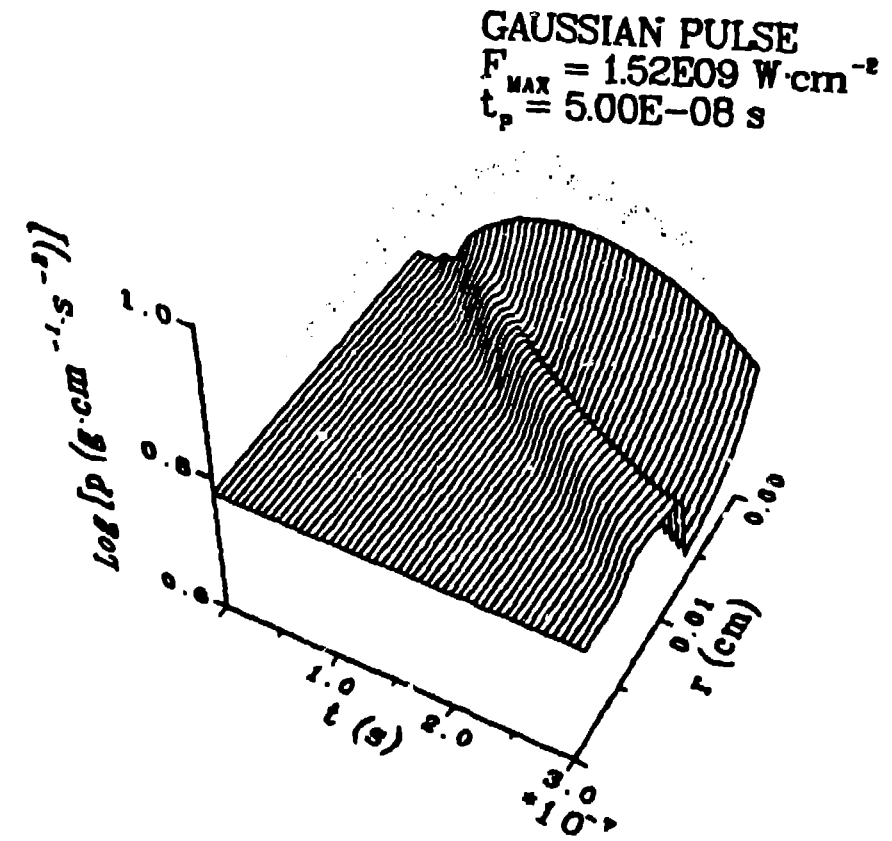

FIGURE 3

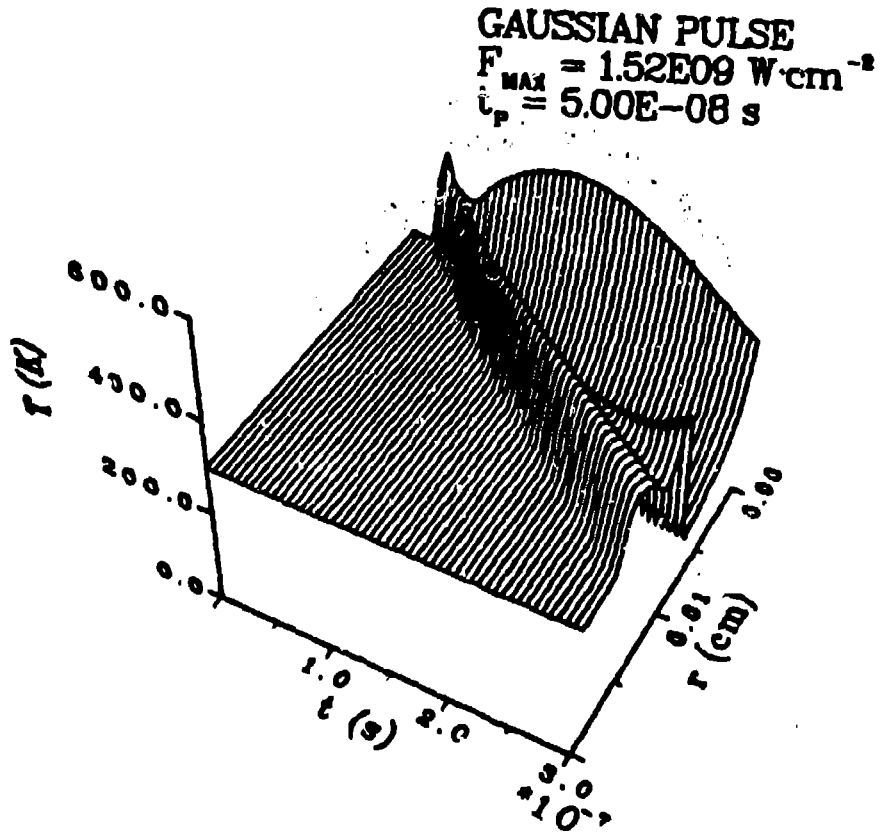

FIGURE 4

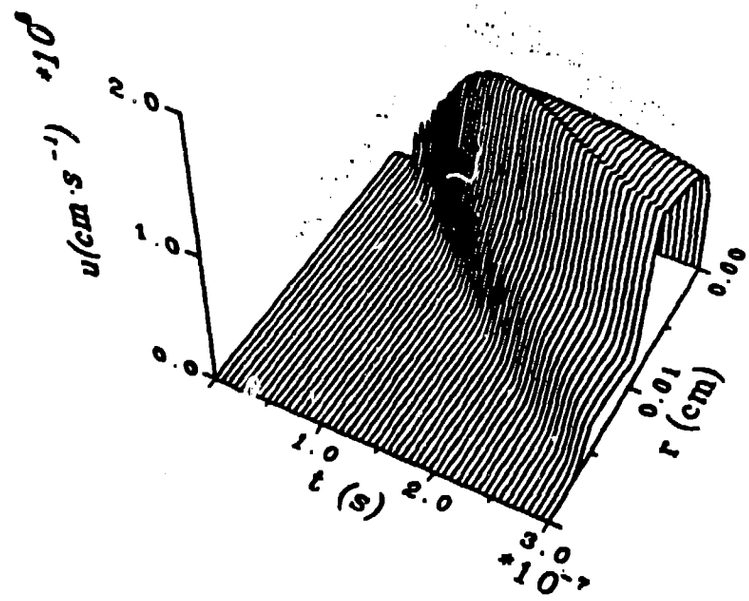

FIGURE 5

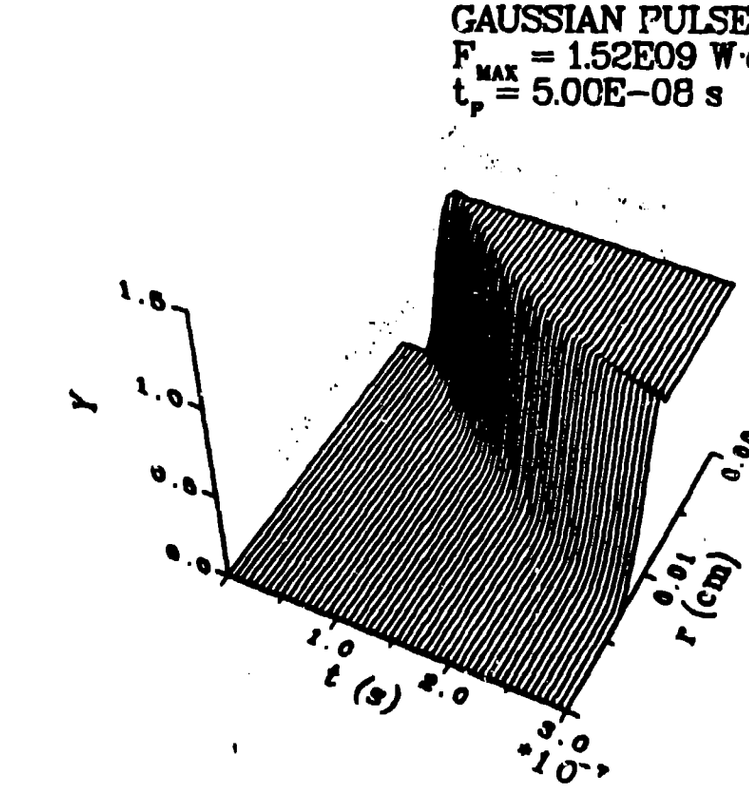

FIGURE 6